Military Technical College
Kobry El-Kobbah,
Cairo, Egypt

6th International Conference
on Electrical Engineering
ICEENG 2008

A Simple Economic Design Strategy for Passenger Hovercrafts and Its Control Algorithm

By

Mohammed A. Kotb, Tarek H. Elsayed, Amr M. Ahmad,
Adel.Rizk, AbdelRaheem M. Deghedy Elsayed Khadrogy *

Abstract:

Passenger hovercrafts present an attractive traveling choice. This is especially true for countries, like Egypt, which rely on tourism as a primary source of income. However, their widespread (and even existence) in many countries is limited due to the high cost as well as the sophisticated technological requirements of the hovercraft design process. These include the expensive prototype model which should be constructed to assess and validate the design calculations as well as the costs involved in constructing the hovercraft and operating it. Moreover, a careful control algorithm is needed to enhance the seakeeping performance of the hovercraft to assure passengers comfort and avoid sea-sickness. In the present paper a simple low cost design approach is proposed and implemented. The proposed strategy has been used to design a hovercraft traveling between Ras Mohammad and Khaleeg Neama in Sharm Elsheikh in Egypt. The proposed model building strategy successfully produces simple cheap prototype models without compromising the accuracy of the design assessment based on them.

Keywords: **hovercraft, control, sea-keeping, Froude scaling, Reynold number.**

*All authors are at Alexandria University, faculty of Engineering

1. Introduction:

Hovercrafts are high speed marine vessels that operate based on the Coanda effect [1]. Fig.1 shows the basic theory of hovercraft operation. The Coanda effect is a phenomenon that allows a fluid jet to remain attached to a wall placed near the fluid jet.

This occurs when a free fluid jet exits a nozzle into an ambient fluid of equal or lower viscosity, which causes entrainment of the ambient fluid. Thus, an air cushion is formed under the vehicle, which helps lift it and which will be used to design high speed marine vehicles. When a wall is placed near the fluid jet, the fluid jet will attach to the wall. The entrainment of the ambient fluid becomes partially blocked by the wall, but continues to be entrained by the jet, thus causing a pressure decrease between the wall and the jet. This pressure difference causes the jet to move towards the wall. If a low pressure separation region and vortex form between the wall and jet, the jet will then attach to the wall. Henri Coanda would later produce multiple patents utilizing the effect he observed and studied to generate propulsion for aircraft. An experiment by Von Glahn found that placing curved and flat plates near a nozzle would result in a ratio of lift to undeflected thrust of about 0.8-0.9, depending on the total deflection angle. Thus a Coanda nozzle could achieve a 90° deflection of the jet-stream and result in a vertical lifting force on the order of 0.8 of the undeflected thrust. This shows that Coanda nozzles can produce lift as well as maintain thrust. The lift is created on the curved surface of the nozzle where the lower pressure regions form. Coanda attempted to use this idea with jet engines to generate flow over outer curved surfaces of crafts he designed. His patent for a lenticular craft give possible insight to the uses of the Coanda effect in the area of aircraft propulsion. The generation of this lift principle can also be seen in the experimental work of Jean-Louis Naudin. His Coanda saucer experiment using a simple concave object and high speed airflow over the top of the object shows that a low pressure region is generated above the craft. This low pressure region creates lift and causes the craft to hover. The high speed flow is able to create the low pressure region by remaining attached to the craft as it flows around it Von Glahn found that the ratio of lift to undeflected thrust to be around 0.8-0.9 in experiments using multiple-flat plates and curved surfaces near a nozzle. This proves that lift can be created using a Coanda nozzle as well as general thrust from the nozzle. However, Von Glahn attributed losses in the lift to undeflected thrust ratio to pressure and momentum losses in the real jet stream that are not accounted for in theory, as well as other factors. To calculate the lift of such a craft, the basic principles of aerodynamic forces is used. The pressure distribution on each side of the body is integrated over the area on which it acts. This results in the forces on the body. The lift is the component of the force in the upwards direction. This includes any lift generated by the rotor blades.

Since Egypt relies on tourism as a major source of income, designing a hovercraft for tourists is quite an attractive choice. The present paper discusses such a design based on simple procedures that do not require highly expensive technological facilities. The feasibility of the implementation of such a project is quite promising.

2. Hovercraft Dynamics

The hovercraft dynamics are described by Kirchoff equations [2]:

$$\begin{aligned} J\dot{\omega} &= J\omega \times \omega + Mv \times v + T \\ M\dot{v} &= Mv \times \omega + F \end{aligned} \qquad (1)$$

where J is the sum of inertia and added inertia, ω is the angular velocity vector, M is the added mass, v is the linear velocity vector. F and T are the actuating force and torque, respectively. The '$\times$' indicates Gibbs product

Since these equations require the identification of the vehicle added mass and added inertia which is practically a difficult task, the authors propose the use of a learning controller which does not rely on accurate knowledge of the vehicle dynamics. The controller details are elaborated in a later section.

3. Full Scale Calculations for the Ras Mohammad/ Khaleeg Neema Hovercraft

The calculations included in the present paper are those relevant for power estimation and control purposes. For details of the design calculation from a structural point of view as well as the industrial processes involved in the full-scale fabrication, the interested reader is referred to [3] available at marine engineering department, faculty of engineering, Alexandria university.

The design and main dimensions are as follows: The length is 12 m, the breadth is 6m, The height (including the cushion height) is 5.25. The speed is 35 Knots (17.5 m/sec). The hovercraft is intended to travel between Ras Mohammad and Khaleeg neama in Sharm El-sheikh. The hovercraft would accomodatw 30 passengers (28 passengers and 2 crew members). Taking the approximate weight of one passenger with his luggage to be 100 Kg, while that of one crew member to be 75 Kg, the total weight of the crew + passengers will be equal to 0.15 +2.8 tons. The hovercraft has 28 chairs each of mass 20 Kg. The weight of the thrust and lift system (engine +thrust fan +lift centrifugal fan +auxiliaries) is estimated to be 2 tons. The superstructure is made of fiber glass whose density is 1550 Kg/m^3. Thus, the weight of the superstructure is taken to be 2.5377 tons. The total tank weight is 2.545 tons. The main deck is made of aluminium alloy and weighs 1.98 tons. The buoyancy tank is made of aluminium weighs 2.67 tons. The overall hovercraft weight including, the fuel control room, bathroom and kitchen will be 17.946 tons. Quick estimates of the required for the required thrust power and lift power are 408.1 HP and 375 HP respectively. The quick estimates are verified because

applying the same rationale to find quick estimates for the power required for thrust and lift by the model resulted in estimates that led to a successfully working model.

4. The Proposed Model Building Strategy and Developed Model

Model building for hovercrafts is very important. The model built can be used to estimate the forces on the full-scale hovercraft. These forces will be used in tuning the hovercraft controller off-line (in simulations).

a. Basic Principles of Model Building

Physical model experiments require some form of similarity between the prototype and the model [4]:

- Geometric similarity: The model must have physical dimensions which are uniformly proportional to those of the prototype; it must have the same shape.
- Kinematic similarity: Velocities in the model must be proportional to those in the prototype.
- Dynamic similarity: Forces and accelerations in the model must be proportional to those in the prototype.

These three similarities require that all location vectors, velocity vectors and force vectors in the coincident coordinates of the scaled model and the prototype have the same direction (argument) and that the magnitude of these vectors (modulus) must relate to each other in a constant proportion.

The ratio between the model forces and full-scale forces is given by the following relation [5]:

$$\frac{F_{FS}}{F_{model}} = \frac{\rho_{FS}}{\rho_{model}} \left(\frac{V_{FS}}{V_{model}} \right)^2 \left(\frac{L_{FS}}{L_{model}} \right)^2 \qquad (2)$$

Where F_{FS} is the full-scale force. F_{model} is the force measured for the scaled model. ρ_{FS} is the density of the fluid for the full-scale (real) working environment. ρ_{model} is the density of the fluid used in the experiments involving the scaled prototype. V_{FS} is the velocity for the full-scale case. V_{model} is the velocity used with the scaled model. L_{FS} is the characteristic full-scale length and L_{model} is the characteristic scaled prototype length.

It is nearly impossible to represent all full-scale forces in a model. Instead, a compromise is made. The most common scaling law used for ships and hovercrafts is Froude scaling where Froude number $\frac{V}{\sqrt{gL}}$ is the same for both the model and the full-scale case. The following procedure is adopted to estimate the total drag on the ship based on experiments on the Froude equivalent model [5].

a. The geometric scaling is usually dictated by the dimensions of the available tank in the lab environment. The speed at which the model must be tested is calculated from the following relation:

$$V_{model} = V_{FS}\sqrt{\frac{L_m}{L_{FS}}} \quad (3)$$

The total drag resistance of the model is given by

$$R_{total} = D_A + D_M + D_F + D_{wave} \quad (4)$$

Part of the [5] drag of the model is calculated D_{Fm} and that of the full-scale prototype. D_{FFS} depends on Reynold's number and is calculated based on readily available theoretical formulas. Fig.2 shows the different areas of the prototype, which are used in the drag calculations.

$$RN = \frac{VL}{\upsilon} = 12.13*10^6$$

$$C_f = \frac{0.075}{(\log RN - 2)^2} = 2.9*10^{-3}$$

$$D_{F1} = 0.5*\rho*V^2*tangential\_area*C_f = 111\ N$$

The resistance due to perpendicular areas D_{F2} is calculated similarly by replacing the tangential areas by perpendicular areas and is found to be 9908.2 Newtons. $|D_M$ is the momentum drag , D_{wave} is the wave making resistance and D_A is air drag. The sum of these drag terms can be measured under Froude scaling. We shall call this sum residual drag.

b. The residual drag of the model is estimated to be $R_m = D_m - D_{fm}$, where D_m is the total measured resistance.

c. Estimate the full-scale hovercraft residual drag using :

$$\frac{R_{FS}}{R_{model}} = \frac{\rho_{FS}}{\rho_{model}}\left(\frac{V_{FS}}{V_{model}}\right)^2\left(\frac{L_{FS}}{L_{model}}\right)^2 \quad (5)$$

5. Finally the total drag of the full-scale hovercraft

$$D_{FS} = R_{FS} + D_{FFS} \quad (6)$$

where the skin friction resistance D_{FFS} is calculated from theoretical formulas.

In general, there are two approaches for realizing Froude equivalence between the full-scale prototype and model. The first popular approach favored by the fluid engineering community, is to test the model in water tunnels and towing tanks. In such test facilities, the model is held constant, while the velocity of the flow is controlled. However, for hovercraft, the determination of the total resistance, would require tests in towing tanks as well as in wind tunnels due to the aerodynamic dependence of the vehicle [6]. In

addition to the required high technology facilities, even if available, using such a setting it is not possible to validate the proposed control algorithm, which is one of the main concerns of model building. Note that a quick estimate of the required power for lift and thrust, have been developed by the authors based on available data and theoretical models. However, model based tests are important for visualization of hydro/aerodynamic phenomena associated with such high speed vessels as well as for control scheme verification. For these reasons, the authors choose the second approach to Froude scaling realization which depends on adjusting the speed of the hovercraft itself.

For the full-scale model Froude no. $\mathrm{Fr} = \frac{17.5}{\sqrt{9.8 * 12}} = 1.6$ Thus, since for the model the dimension is scaled from 12 to 0.45 m, the velocity should be 3.4 m/s instead of 17.5 m/s, to maintain the Froude equivalence. Thus, experiments on the model can be used to verify the control algorithm as well as to estimate (without exaggeration) the total drag of the full-scale prototype.

To estimate the power required to lift the full-scale model, the following calculations are used. The cushion pressure is found from the craft mass and cushion area. $P_C = \frac{\mathrm{Mass} * g}{\mathrm{area}} = \frac{2000 * 9.8}{12.77 * 6.48} = 2371\,\mathrm{Pa}$.

The cushion parameter is $\mathrm{CPc} = \frac{2a}{h(1+\cos\theta_s)}$ where a is the gap between the buoyancy tank and the skirt and h is the lift height. The cushion The lift power is $P_{\mathrm{lift}} = P_c^{2/3}\sqrt{\frac{2}{\rho}}h * \mathrm{CP}_c = 282.04\,\mathrm{KW}$, Thus, the required lift power is 375 HP.

b. Model Building Strategy

Fig. 3 shows the steps of model building. The scale is chosen to be 1:26. The speed should be 3.4 m/sec to maintain Froude equivalence.

Model length is 45 cm, breadth is 27 cm, while depth is 15 cm (with skirt). Hover height =7 mm. The model building procedure is as follows:

1. First, the model base (45 cm x 27 cm) is made from plywood.
2. The buoyancy tank is made from foam (42 cm x 24 cm).
3. The buoyancy tank is attached to the base through supports made from foam.
4. The skirt is cut in accordance with base dimensions and is then attached to the base with the buoyancy tank.
5. The lift motor and lift fan are fixed to the base.
6. The thrust motor and the thrust fan are then attached to the base.
7. The motors are connected to the power supply.

8. The body of the hovercraft is installed at the base.

A quick estimate for calculating the required thrust and lift power for the model is as follows: To estimate the required thrust power, it is important to calculate an overall estimate of the model drag. Since, the friction drag is the major drag component, the residual drag may be taken as a percentage of it. Fig.4 shows the main areas used to calculate the drag:

$A_1 = 0.16 * 0.045\,m^2$, $A_2 = 0.16 * 0.05\,m^2$, $A_3 = 0.16 * 0.02\,m^2$,

$A_4 = 0.34 * 0.075 * 2(\text{for 2 sides})\,m^2$, $A_5 = 0.16 * 0.02\,m^2$,

$A_6 = 0.45 * 0.05 * 2(\text{for 2 sides})\,m^2$, $A_7 = 0.12 * 0.085\,m^2$

The tangential areas are $A_3 + A_4 + A_5 + A_6 = 0.1312\,m^2$. The perpendicular areas $A_1 + A_2 + A_7 = 0.0254\,m^2$. The Reynold dependent friction drag is calculated using the formulas depicted in the previous section and is found to be $1.4 * 10^{-3}$ for tangential areas and 0.045 for perpendicular areas 0.045. Thus, the total resistance is 0.0464 (all forces are in Newton). The residual resistance is taken as a portion of it. The power is thus calculated as the product of the model resistance times the model velocity and is found to be 0.81 HP

The lift power is estimated in a similar fashion to the previous sections lift power full-scale estimation and is found to be 0.0874 HP

6. ***The Proposed Control Scheme***

a. Challenges of Hovercraft Control (steering and ride control)

The hovercraft is a fascinating ground vehicle that possesses the unique ability to float above land or water. Riding on a cushion of air endows the hovercraft with many interesting and useful properties. Unlike wheeled robots which feature constrained kinematics, the hovercraft can move freely in any direction. For example, although the lateral direction of travel is not usually actuated, the hovercraft is completely free to move sideways. In addition, the frictional damping force acting on a hovercraft is minimal. For autonomous hovercraft applications, the lack of friction places an additional burden on the controller, as all velocity damping forces must be created by the actuators. The combination of the rich hovercraft dynamics and minimal frictional damping make the automatic control of a hovercraft a complex and interesting problem. As has been pointed out earlier, the hovercraft achieves lift by creating a volume of high pressure air underneath the vehicle. A skirt made from flexible material encircles the underbody of the vehicle and prevents the high pressure air from rapidly escaping the plenum when the hovercraft lifts above the ground. A properly designed skirt is crucial to vehicle stability and ride comfort. The skirt must be flexible so that it conforms to uneven terrain, durable enough to prevent abrasion and tearing, and lightweight. For

these reasons, the skirt is the most critical aspect of the entire hovercraft design. A hovercraft achieves lift and propulsion by one or more high-power fans. Steering and vehicle control may be achieved in various ways. On some hovercraft, the fans may be swiveled a full 360 degrees to produce thrust in any direction. Using two fans inline with the vehicle center of mass allows a hovercraft to turn in place simply by running the fans in opposite directions. An alternative actuation approach is to use a fixed fan and a rudder to steer. The thrust fan is usually shrouded by a duct for greater thrust efficiency, and the rudder is located in the high velocity air stream. A rudder steering mechanism adds considerable complexity to the vehicle control. First, the fan must produce sufficient air speed for the rudder to be effective as a control surface. Thus, any turning maneuver is always accompanied by a forward (or reverse) thrust component. As a result, a hovercraft with a rudder cannot generate a pure torque and is thus unable to turn in place. Second, the rudder is mechanically limited and cannot produce force directed along the hovercraft's lateral direction. For these reasons, a hovercraft with a rudder is an underactuated system and an interesting problem for automatic control. Despite increased control difficulty, underactuated systems can provide a substantial savings in actuator cost, size, and weight, and may be the only viable option for many applications. The control and stabilization of underactuated vehicles, however, can be quite challenging. Difficulties arise because classical nonlinear control techniques, such as feedback linearization, are not always applicable for underactuated systems. Other traditional methods such as linearization and gain scheduling are popular due to their simplicity, but guarantee stability for only a local neighborhood of the operating point. Moreover, a linear controller will often perform poorly whenever the nonlinear modes of the system are exercised. A traditional approach to trajectory tracking uses the linearization of the system dynamics about a nominal state space trajectory. The problem is that the formulation of feasible state space trajectories can be particularly difficult for vehicles with complex dynamics. For example, certain circular trajectories with rigid heading constraints are not physically realizable by our hovercraft's dynamics. Even in cases where the hovercraft is not underactuated, still traditional control methods may not be applicable due to the difficulty to obtain an accurate model of the hovercraft. This favors model independent approaches.

Controlling the hovercraft seakeeping behavior as a ride control system is another major challenge [7]. Ride control systems have become an integral feature of most fast ferries. The development of these systems has required a continuous joint international development effort involving builders, operators, and suppliers. In the early days, it was believed that larger vessels and sophisticated hull forms would completely alleviate motion problems. However, the operating profile of fast ferries requires operation at high speed in high waves to maintain schedule. It was discovered that passengers, hull structure, and shipboard machinery were adversely affected by the motions encountered when these groundbreaking vessels ventured into previously untried conditions.

Builders and operators continue to play a key role in the improvement of ride control systems. Passenger comfort is very important. An entire family can be lost from an operator's potential customer base if one member of a family becomes seasick.

To summarize, it is desirable to use a hovercraft controller that can track a desired trajectory while maintaining favorable sea keeping behavior. It should be model independent.

b. The Proposed Model Independent Controller

As opposed to traditional control approaches which are model dependent, the present paper proposes the use of a model-independent Fourier learning controller. The Fourier learning controller has been used successfully to cope with unknown/ partially known nonlinear systems [8],[9]. To learn a certain trajectory, the hovercraft can be considered to be implicitly repeating the same task several times (for the different time steps). Thus, a desired path can be approximated by a sequence of waypoints. Within each segment the learning controller is applied at fixed time steps. The advantage of Fourier learning controller over other learning controllers is that it is guaranteed to converge even (and especially) when each step is repeated from a different initial condition. Thus, the tracking of each line segment of the desired path may be attempted at discrete time steps. The performance (capability of tracking the desired path) improves since it adapts its behavior based on its error in the previous iterations (time steps). This periodic nature of the learning controller motivated Tang et al. [9] to use Fourier series as a basis of their controller. Consider the following. The controller of the system i in the kth cycle has the following form (The following equations are for the steering angle. Similar equations can be readily derived for the x and y cases):

$$\begin{aligned} \tau_{ik}(t) &= (PD)_{ik} + \tau'_{ik}(t) \\ &= k_{vi}\Delta\dot{\theta}_{ik}(t) + k_{pi}\Delta\theta_{ik}(t) + \tau'_{ik}(t) \end{aligned} \tag{8}$$

Where k_{vi} and k_{pi} are positive constant feedback gains. $\theta_{ik}(t)$ and $\Delta\theta_{ik}(t)$ are the output angular error and angular velocity error of system i in the kth cycle, respectively, and τ'_{ik} is the estimation of the optimal feedforward τ_i^*. Similar control laws can be deduced for linear position.

Substituting into and applying Fourier transform on both sides of the above equation, we obtain

$$\frac{a_{i0k}}{2} + \sum_{n=1}^{N_i}\left(a_{ink}\cos n\omega_i t + b_{ink}\sin n\omega_i t\right)$$

$$= \frac{p_{i0k}}{2} + \sum_{n=1}^{N_i}\left(p_{ink}\cos n\omega_i t + q_{ink}\sin n\omega_i t\right) + \frac{a'_{i0k}}{2} \qquad (9)$$

$$+ \sum_{n=1}^{N_i}\left(a'_{ink}\cos n\omega_i t + b'_{ink}\sin n\omega_i t\right)$$

The left-hand side represents the dynamic system, and the right-hand side represents the controller output or input torque. a_{ink} and b_{ink} are the projection of system i on the nth harmonic frequency. They are determined by the system function

$$a_{ink} = \frac{2}{T_i}\int_{(k-1)T_i}^{kT_i} f_{\tau_i}(.)\cos n\omega_i t \; dt \qquad (10)$$

$$b_{ink} = \frac{2}{T_i}\int_{(k-1)T_i}^{kT_i} f_{\tau_i}(.)\sin n\omega_i t \; dt \qquad (11)$$

p_{ink} and q_{ink} are calculated from PD controller output

$$p_{ink} = \frac{2}{T_i}\int_{(k-1)T_i}^{kT_i} (PD)_{ik}\cos n\omega_i t \; dt \qquad (12)$$

$$q_{ink} = \frac{2}{T_i}\int_{(k-1)T_i}^{kT_i} (PD)_{ik}\sin n\omega_i t \; dt \qquad (13)$$

a'_{ink} and b'_{ink} will be generated by the learning controller. Hence, the closed-loop system dynamics equations in Fourier space is obtained and written as

$$a_{ink} = p_{ink} + a'_{ink} \qquad (14)$$

$$b_{ink} = q_{ink} + b'_{ink} \qquad (15)$$

Since the real part and imaginary part of Fourier series have similar characteristics, hereafter we use a_{ink}, a'_{ink}, and p_{ink} to represent the $(2N_i + 1)$ Fourier coefficients of $\tau_{ik}(t)$, $\tau'_{ik}(t)$, and $(PD)_{ik}$ when no confusion is caused. The controller design task is to develop an algorithm for a'_{ink} to force a'_{ink} and a_{ink} to approach the same value, which is the corresponding Fourier coefficient of the optimal feedforward $\tau_i^*(t)$. So, in time domain $\tau'_{ik}(t)$, and $\tau_{ik}(t)$ will converge to the same function $\tau_i^*(t)$, and $(PD)_{ik}$ will approach zero simultaneously. Then, the output error $e_{ik}(t)$ will asymptotically

converge, since $(PD)_{ik} = 0$ constructs a stable sliding surface. From the above equations it can be noted that the PD Fourier coefficients represent the error in the estimate of the Fourier coefficients of the optimal torque. Thus, according to the idea of PI (proportional-integral) regulator, $e(t) + k_i \int e(t)$ can force the system output to approach a constant setting point. Accordingly, a suitable a update-law is

$$a'_{ink} = \gamma_{in} \sum_{j=0}^{k-1} p_{inj} \qquad (16)$$

With gain $\gamma_{in} > 0$. Then the closed-loop system dynamics equation in Fourier space is

$$p_{ink} + \gamma_{in} \sum_{j=0}^{k-1} p_{inj} = a_{ink} \qquad (17)$$

Algorithm Outline

Given Conditions: The sampling period ΔT_i. The desired $\theta_i^d(t)$, $t \in [0, T_i]$, or $\theta_i^d[j]$, $j = 1,2,..., M_i$ with $M_i = (T_i / \Delta T_i)$.

Step 0) Search PD controller gains to stabilize the controlled system with acceptable tracking performance.

Set $a'_{ink} = 0$ and $b'_{ink} = 0$ for all i and n. Set the learning counter $k = 1$.

Step 1) Set sampling counter $j = 1$, $p_{ink} = 0$, and $q_{ink} = 0$.

Set the learning gain γ_{in}.

Step 2) Calculate the compensation term

$$comp[j] = \left(a'_{i0k} / 2\right) + \sum_{n=1}^{N_i} \left(a'_{i0k} \cos(n(2\pi / M_i)j) + b'_{i0k} \sin(n(2\pi / M_i)j)\right).$$

Apply PD controller to the plant and get $\Delta\theta_{ik}[j] = \theta_i^d[j] - \theta_{ik}[j]$,

$(PD)_{ik}[j] = k_{pi}\Delta\theta_{ik}[j] + k_{vi}\Delta\theta_{ik}[j]$. System input $u = (PD)_{ik}[j] + comp[j]$.

After each sampling, increase j by 1 (i.e., $j \to j+1$) and calculate

$p_{ink} \to p_{ink} + 2/M_i (PD)_{ik}[j] \cos(n(2\pi / M_i)j)$,

$q_{ink} \to q_{ink} + 2/M_i (PD)_{ik}[j] \sin(n(2\pi / M_i)j)$.

Step 3) If $j \neq M_i$, continue step 2).

Step 4) If the error index in the kth trial $EI_k < \varepsilon$ (learning process ends), go to step 1).

Step 5) Calculate $a'_{in(k+1)} = a'_{ink} + \gamma_{in} p_{in}$, $b'_{in(k+1)} = b'_{ink} + \gamma_{in} q_{in}$.

Increase k by 1 (i.e., $k \to k+1$) and go to step 1).

A sufficient but not necessary condition to ensure the controller convergence is: $0 < \gamma_{in} < 1$, and the closed-loop system I/O relation in Fourier space satisfies $\left|(\Delta a_{ink} / \Delta p_{ink})\right| < 1 - \gamma_{in}$ for all i and k, where $\Delta a_{ink} = a_{in(k+1)} - a_{ink}$, $\Delta p_{ink} = p_{in(k+1)} - p_{ink}$ Fig. 5 shows how the Fourier learning controller successfully tracked a desired path defined in terms of a starting point, ending point and desired velocity. The figure shows the sum-squared error in all degrees of freedom along the whole time record. It is clear that the error falls quite rapidly, especially after the first learning iteration. The control signals required for feedback can be easily provided using a conventional inertia navigation system.

6. Conclusions

The contribution of the present research is summarized as follows. Although a hovercraft for tourists is quite a promising project for Egypt, it was considered before to be infeasible. This is due to the fact that the expenses of buying a hovercraft to directly deploy it is quite high. In addition to that building the design in Egypt was considered difficult. This is because the practical details that must be unraveled to fully implement the hovercraft in house are not readily available in literature. This is especially true due to the complicated dynamics of the hovercraft system which involves both aerodynamic and hydrodynamic complexities. Building a working hovercraft prototype is thus far from being an easy task. There must be a means to verify the initial design estimates before carrying them out on the full-scale prototype. This is precisely the contribution of the present research. The authors successfully built a working hovercraft model that has three major benefits. First, since the authors approximate calculations successfully resulted in producing a working model, then it is possible to use them even at the full-scale to obtain a working prototype. Second, provided that Froude equivalence is maintained between the model and prototype is made, measurements may be performed to obtain a more accurate estimate of the full-scale drag without having to use a high factor of safety. In addition to these advantages, it is possible to use the model to verify the proposed control algorithm. The contribution of the proposed control algorithm is that it alleviates the need for expensive and tedious system identification experiments. The learning controller can be tuned using the practical model and Froude equivalence can be used to find the forces and torques required by the full-scale prototype to track a certain path. Using several pre-calculated stored motion primitives can be used to successfully approximate any desired path while maintaining favorable seakeeping behavior. This is important to assure tourists comfort and enjoyment of the hovercraft ride.

7. Acknowledgement

Thanks to Allah the most merciful and gracious for helping us with this project that we hope to prove to be quite beneficial for Egypt economy. The faculty staff at the marine engineering department has been quite encouraging. We would like to pay special

respect to the memory of our colleague Tarek Elsayed who has been a dear member of the project. We hope God would reward him eternally for his precious efforts to bring this project to light.

References

[1] E. A. Kelleher, *A Study of a Skirtless Hovercraft Design*, Master of Science Dissertation, The Faculty Department of Aeronautics and Astronautics, Graduate School of Engineering and Management Air Force Institute of Technology, Air University, Air Education and Training Command, Ohio, U.S.A, May 2004.

[2] Z. Kulis, *Feedback Control of a Hovercraft over a Wireless Link*, Master of Science, Department of Electrical and Computer Engineering, Institute for Systems Research, 2006.

[3] A. Rizk, T. Elsayed, A. Deghedy, A. Abouzeid, *Passengers Hovercraft*, BSc. Honors Thesis, Marine Engineering Department, Faculty of Engineering, Alexandria University, Egypt, May 2007

[4] J.M.J. Journée and W.W. Massie, *Offshore Hydromechanics*, Delft University of Technology, lecture notes, http://www.shipmotions.nl/LectureNotes.html.

[5] J. Douglas, J. Gasiorek, *Fluid Mechanics*, Longman, England 1985

[6] J. Harris and S. Grilli, *Computation Of The Wavemaking Resistance Of A Harley Surface Effect Ship.*Proc. 17th Offshore and Polar Engng. Conf., ISOPE07, Lisbon, Portugal, July 2007

[7] *Making Passengers Comfortable*, Incat The Magazine Vol.2 Issue 4, article available online.

[8] H. Attia, A. Saber, M. Haleem, *A New Simple Approach To Biomimetic Automated Underwater Vehicles Design*, International conference of Mechanical Design and Production, MDP9, Cairo, Egypt, 2008

[9] Xiaoqi Tang, Lilong Cai, and Weiqing Huang, *A Learning Controller for Robot Manipulators Using Fourier Series*, IEEE Transactions on Robotics and Automation, Vol. 16, no. 1, February 2000

[10] Malcolm A. MacIver, Ebraheem Fontaine, and Joel W. Burdick, *Designing Future Underwater Vehicles: Principles and Mechanisms of the Weakly Electric Fish*, IEEE Journal of Oceanic Engineering, Vol. 29, no. 3, July 2004

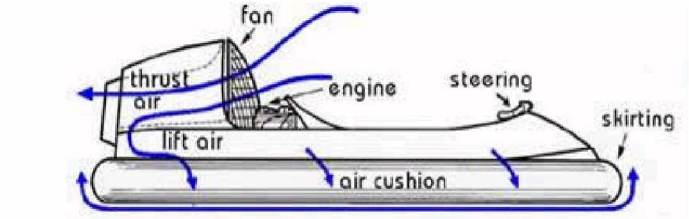

Figure (1): *The basic principles of hovercraft operation A fan is usedto introduce a layer of air between water surface and the vehicle, thus reducing frictional resistance.*

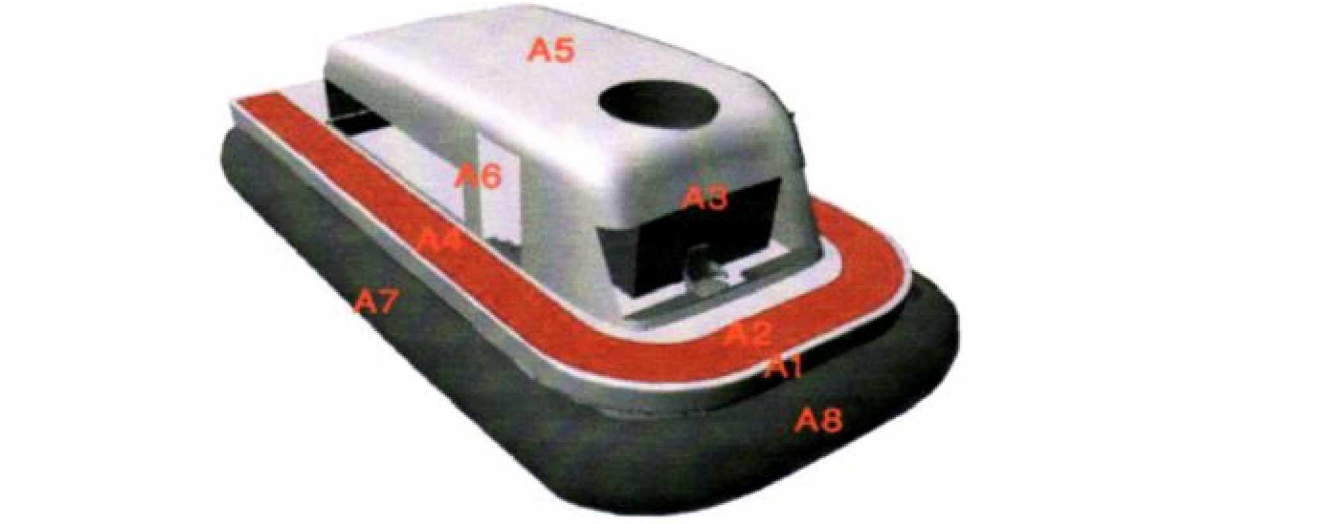

Fig. 2 The different areas of the full scale prototype that are involved in drag calculations.

Figure (2): *The different areas of the full-scale prototype involved in the drag calculations*

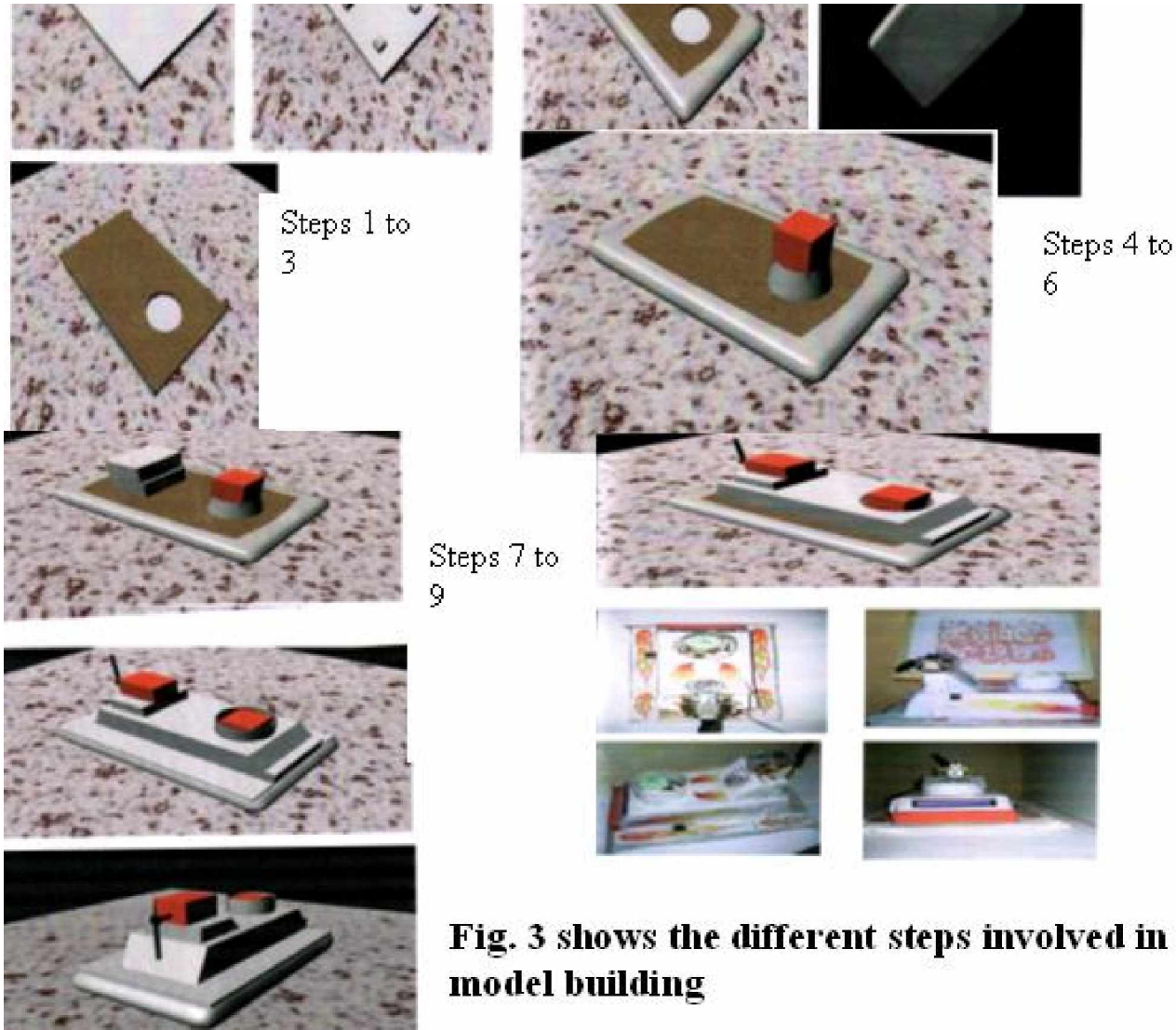

Fig. 3 shows the different steps involved in model building

Figure (3): *The different steps of building the model*

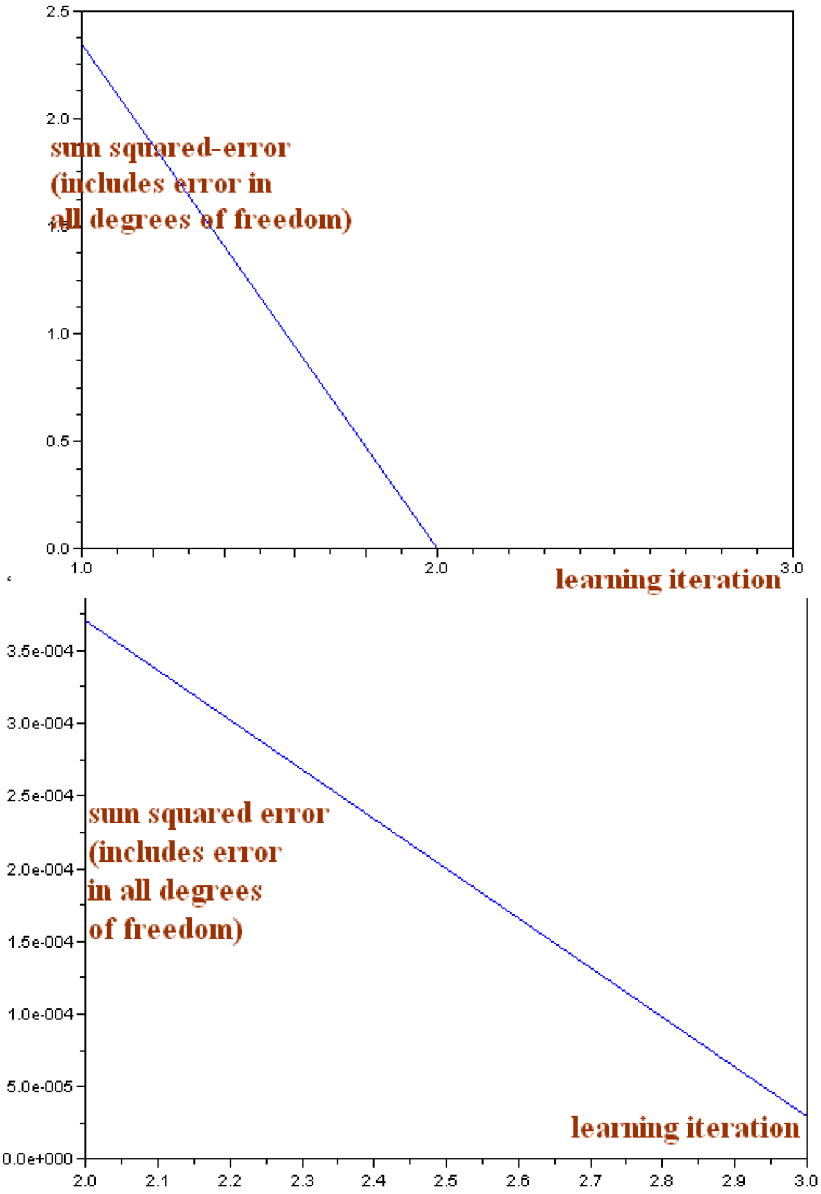

Figure (5): *The Fourier learning controller error while tracking a desired location. Note that because the error falls greatly after the first iteration, we had to plot the error progress in further iterations in a separate plot.*